

SPATIAL DIFFUSION OF STARS IN THE INNER GALACTIC BULGE

SUNGSOO S. KIM & MARK MORRIS

Division of Astronomy & Astrophysics, University of California, Los Angeles, CA 90095-1562;
sskim@astro.ucla.edu, morris@astro.ucla.edu

To appear in ApJ, Jun 2001 issue

ABSTRACT

Star formation in the inner few hundred pc of the Galactic bulge occurs in a flattened molecular layer called the central molecular zone (CMZ). Serabyn & Morris (1996) suggest that the star formation in the CMZ has been sustained for the lifetime of the Galaxy, and that the resulting agglomeration of stars formed in the CMZ has resulted in the prominent r^{-2} stellar density cusp at the Galactic center having about the same physical extent as the CMZ. This “central cusp” is somewhat less flat than the CMZ; thus the population of stars formed in the CMZ appears to have diffused out to larger latitudes. We hypothesize that such vertical diffusion is driven by the scattering of stars off the giant molecular clouds (GMC) in the CMZ, and perform numerical simulations of the scattering between stars and GMCs in the presence of the non-axisymmetric background potential. The simulation results show that the time scale for an initially flattened stellar population to achieve an aspect ratio of the observed OH/IR stars in the inner bulge, 1 to 2 Gyr, agrees well with the estimated age of those OH/IR stars.

Subject headings: celestial mechanics, stellar dynamics — Galaxy: center — Galaxy: kinematics and dynamics
— methods: numerical

1. INTRODUCTION

It has long been known that the central bulge of the Galaxy has a distinct stellar density profile which approximately follows an r^{-2} law (Becklin & Neugebauer 1968). This r^{-2} cusp has often been assumed to be merely the innermost part of the elderly bulge (Evans & de Zeeuw 1994, among others). However, the fact that the Central Molecular Zone (CMZ) has the same maximum identifiable extent in Galactic longitude as this stellar cusp (~ 200 pc) led Serabyn & Morris (1996) to propose that star formation has been steadily occurring in the CMZ throughout the lifetime of the Galaxy.

The CMZ is a massive reservoir of molecular clouds unparalleled in the Galaxy. It is an active region of star formation with a number of very young stellar clusters and ample ionized gas occupying the central ~ 400 pc \times 100 pc region ($l \times b$; see Figure 1). The clouds within the CMZ have relatively high density ($n \gtrsim 10^4$ cm $^{-3}$), high volume filling factor ($f \gtrsim 0.1$), and significantly elevated temperatures (30–200 K, typically ~ 70 K; Hüttemeister et al. 1993, among others), and their total mass is estimated at $5 - 10 \times 10^7 M_{\odot}$ (Serabyn & Morris 1996), representing roughly 10% of our Galaxy’s neutral gas content. The inevitable angular momentum loss in an orbiting gas disk results in gas inflow along the Galactic plane from the outer bulge to the CMZ. Serabyn & Morris enumerate the mechanisms for the angular momentum loss as follows: 1) shear viscosity in the differentially rotating gas disk, 2) shocks associated with a bar potential, 3) cloud-cloud collisions, 4) dynamical friction of giant molecular clouds by field stars (Stark et al. 1991), 5) magnetic field viscosity (Morris 1996), and 6) dilution of specific angular momentum by stellar mass loss material raining down out of the slowly rotating Galactic bulge (Jenkins & Binney 1994).

Both the stellar population (r^{-2} cusp) and the CMZ are considerably flattened along the Galactic plane. While the aspect ratio of the bulge is 1.6–1.7 (Kent, Dame, & Fazio 1991; Weiland et al. 1994), those of the stellar population and the CMZ are ~ 2.2 (Catchpole, Whitelock, & Glass 1990) and ~ 4 (Serabyn & Morris 1996), respectively. The mass of the stellar

population within the ~ 100 -pc extent of the CMZ, $\sim 10^9 M_{\odot}$, falls near the lower end of the range predicted for the stellar mass emerging from the CMZ over the Galaxy’s lifetime, and Serabyn & Morris consider this as additional support for the association between the stellar population and the CMZ.

Here we focus our attention on the difference of the aspect ratios between the r^{-2} stellar population and the CMZ. In the context of the sustained star formation hypothesis, one may interpret the observation that the aspect ratio of the stellar population is smaller than the CMZ in terms of the vertical diffusion of stars formed in the flatter CMZ by gravitational perturbations.

The vertical heating of the stars born in the Galactic disk due to gravitational perturbations has been studied by many authors, especially for heating by giant molecular clouds (GMCs). Spitzer & Schwarzschild (1951, 1953) first proposed that random encounters of the stars formed in a thin disk with massive interstellar clouds would heat up the stellar populations (the presence of GMCs was not known until ~ 20 years later). They used a Fokker-Planck model to calculate the evolution of the velocity dispersions. Lacey (1984) performed similar calculations but with a consideration of vertical motions of stars. Villumsen (1983, 1985) approached the same problem by integrating the equation of motion for a tracer population of non-self-gravitating stars evolving in the gravitational fields of the fixed background (disk and halo) and of the GMCs. On the other hand, Barbanis & Woltjer (1967) proposed that transient spiral density waves could heat up the stellar populations. A series of papers (Carlberg & Sellwood 1985; Carlberg 1987; Sellwood & Kahn 1991) has explored this mechanism numerically. However, neither of the above two mechanisms alone was able to explain the observations. The models involving scattering by the GMCs predicted the ratio of stellar velocity dispersions perpendicular to the plane and towards the Galactic center, σ_z/σ_R , to be larger than that observed. They also predicted that the velocity dispersion increases with time as $\sim t^{0.25}$, which is substantially slower than implied by the observations, $\sim t^{0.5}$ (Wielen 1977). Meanwhile, spiral structure was found to be highly inefficient in increasing σ_z . Thus, both mechanisms

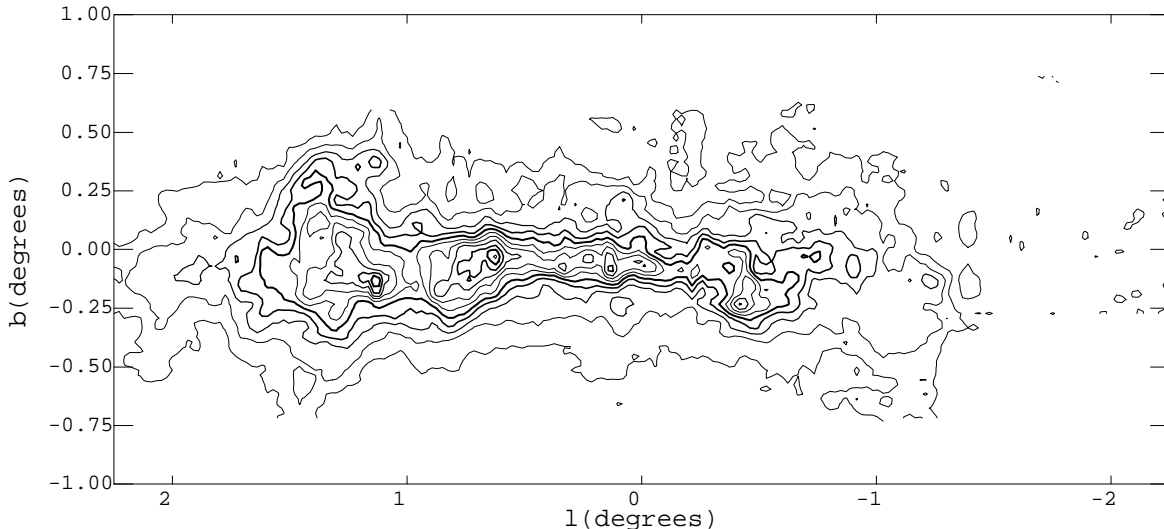


FIG. 1.— Integrated intensity of ^{12}CO , $J = 1-0$ emission, from the AT&T Bell Labs survey of the inner Galactic bulge region (Uchida, Bally, & Morris, unpublished work). Contour lines were drawn at intervals of $250\text{K} \cdot \text{km s}^{-1}$, starting from $250\text{K} \cdot \text{km s}^{-1}$.

needed to be considered to account for the observations, and the study of the stellar heating under the combined influence of both GMCs and spiral structure was made by Jenkins & Binney (1990), whose simulations were found to agree with observations of spiral structure material near the Sun.

Contrary to the case of the Galactic disk, the kinematic evolution of a population of stars formed in the CMZ via heating processes has not been studied. The kinematic environments in the inner bulge differ from those in the disk mainly in three respects: 1) the background gravitational potential in the inner bulge is neither axisymmetric nor plane-parallel; 2) the presence of density waves strong enough to significantly heat the stellar population seems unlikely (weakly damped modes may be present though; see, e.g., Weinberg 1994); and 3) the dynamical time scale in the inner bulge is considerably shorter than in the disk. Because of 1), we may not apply the analytic study of the kinematic evolution of the disk stars directly to the inner bulge. In the present paper, we hypothesize that the stellar population formed in the CMZ diffuses mainly by scattering off the GMCs and we study the kinematic and spatial evolution of stars in a flattened configuration by following the trajectory of non-self-gravitating particles under the gravitational potential of the background (inner bulge and nucleus) and the GMCs, similarly to the work by Villumsen (1985) for the case of the Galactic disk. We choose to approach this problem numerically, in order to obtain more tangible results.

If the scattering off the GMCs causes the stellar population to diffuse out from the inner bulge faster than the rate at which stars are formed in the CMZ, the resulting stellar population would have a significantly larger extent than the CMZ, instead of forming a configuration having a scale similar to the CMZ, such as the r^{-2} stellar population that we currently observe. On the other hand, if the diffusion is highly inefficient, the resulting stellar population from the sustained star formation in the CMZ would have a configuration very similar to that of the CMZ. Since the time scale of the stellar diffusion in the inner bulge is an important parameter, the calculation of the vertical evolution of the stellar population and its comparison with observations are essential for assessing our hypothesis. We compare our simulation results with the distribution of OH/IR stars, one of few

object categories in the inner bulge that currently provides approximate information on the age.

Our simulation models are described in § 2. We show and discuss our results in §§ 3 and 4. Finally, our findings are summarized in § 5.

2. MODELS

As discussed in § 1, the background potential in the inner bulge is neither axisymmetric nor plane-parallel, which complicates any analytic approach for the kinematic evolution of stars within it. We therefore study the problem by directly integrating the orbital motion of non-self-gravitating test particles. The total integration time of our simulations is either 1 or 3 Gyr. Our model parameters discussed below are given in Table 1.

2.1. GMCs

Many groups have conducted radio observations of molecular clouds in the inner bulge (see Morris 1997 for a list of such observations). Here, for the GMC parameters in our simulations, we adopt a CO line survey by Oka et al. (1998). They identified $\gtrsim 15$ molecular clouds with a size of ~ 30 pc and obtained a total molecular mass in all clouds of $\sim 4 \times 10^7 M_{\odot}$. We take 20 for the number of GMCs, N_{GMC} , and 2.5×10^7 or $5 \times 10^7 M_{\odot}$ for the total mass in GMCs, M_{GMC} . For the sake of simplicity, a Plummer model is adopted for the potential by the GMC:

$$\Phi_{\text{GMC}} = -\frac{Gm_{\text{GMC}}}{(d^2 + \epsilon_{\text{GMC}}^2)^{1/2}}, \quad (1)$$

where m_{GMC} is the mass of a GMC, ϵ_{GMC} the core radius of the Plummer model, and d the distance to the GMC. Considering the size of the GMCs in the inner bulge, we use ϵ_{GMC} of 5 or 10 pc.

Since only the projected positional distribution and the line-of-sight velocity of the GMCs are available, the three-dimensional positional and velocity distribution of GMCs must be assumed. We assume that the R (galactocentric radius projected onto the Galactic plane; note that we use r for the three-dimensional galactocentric radius and l for the projection of R onto the plane of the sky) distribution ranges from 10 to 150 pc

TABLE 1
MODEL PARAMETERS FOR DIFFUSION SIMULATIONS

Model	Ω_p ($\text{km s}^{-1} \text{kpc}^{-1}$)	M_{GMC} (M_\odot)	α_{GMC}	ϵ_{GMC} (pc)	α	Φ_0 ($\text{pc}^2 \text{G}^{-1} \text{Myr}^{-2}$)	z_0
1	65	2.5×10^7	-1	10	-1.8	3.1×10^4	0.8
2	65	2.5×10^7	-1	10	-1.8	3.1×10^4	0.7
3	65	2.5×10^7	-1	10	-1.5	4.5×10^3	0.8
4	65	2.5×10^7	-1	10	-1.8	7.8×10^4	0.8
5	50	2.5×10^7	-1	10	-1.8	3.1×10^4	0.8
6	65	5.0×10^7	-1	10	-1.8	3.1×10^4	0.8
7	65	2.5×10^7	0	10	-1.8	3.1×10^4	0.8
8	65	2.5×10^7	-1	5	-1.8	3.1×10^4	0.8

NOTE.—Model 1 is our standard model. Variations from model 1 are denoted by boldfaces. For all models, $\sigma_{v,xy} = 20 \text{ km s}^{-1}$, $\sigma_{v,z} = 25 \text{ km s}^{-1}$, $N_{GMC} = 20$, $y_0 = 0.9$, and $a_0 = r_0 = 1 \text{ pc}$.

and that the surface number density varies as $R^{\alpha_{GMC}}$. Binney et al. (1991) proposed that GMCs inside the 180-pc molecular ring move along the so-called X_2 orbits (Contopoulos & Mertzaniides 1977) and are gradually transported inward at a constant velocity due to angular momentum loss. Since the gas is thought to flow inwards along the Galactic plane, if the gas is transported inward while conserving its mass, α_{GMC} is required to be -1 . We here try $\alpha_{GMC} = -1$ and 0 . The inward migration takes place on a time scale much longer than that of the X_2 orbital motion, thus we neglect the inward migration and assume that the GMC motions in the plane follow X_2 orbits. We also assume that the CMZ maintains the same properties over the entire computational time interval.

The information on the motion of GMCs along the z -axis and its dependence on R are very limited. Therefore we assume that the vertical velocity dispersion of the GMCs, $\sigma_{v,z}^{GMC}$, is constant over R and simply impose a sinusoidal vertical motion to the GMCs with an amplitude $H_{GMC}(R)$ that corresponds to the adopted $\sigma_{v,z}^{GMC}$. Under the standard background potential adopted below, the X_2 orbital motion with $\sigma_{v,z}^{GMC} = 25 \text{ km s}^{-1}$ gives H_{GMC} nearly proportional to R , with $H_{GMC} \simeq 25 \text{ pc}$ at $R = 150 \text{ pc}$. We use $H_{GMC} = 25 (R/150 \text{ pc}) \text{ pc}$ in the simulations. For comparison, the 15 giant molecular clouds observed by Oka et al. (1998) have an average z -distance of 18 pc, and Oka et al. estimate $\sigma_{v,z}^{GMC}$ to be $\gtrsim 32 \text{ km s}^{-1}$. The initial positions of the GMCs are randomly chosen, but follow the assumed radial distribution, $R^{\alpha_{GMC}}$, and GMCs are assumed not to interact with each other. In order to lessen the CPU burden, we pre-calculate the X_2 orbit of each GMC and save it in a table. Then, when the equation of motion for the stars is integrated, the x - y position of each GMC at a given time is obtained from the table and the z position is obtained from the sinusoidal motion with period $4H_{GMC}/\sigma_{v,z}^{GMC}$, and with $\sigma_{v,z}^{GMC} = 25 \text{ km s}^{-1}$.

2.2. Background Potential

We model the potential of the inner bulge as

$$\Phi = \Phi_0 \left(1 + \frac{a}{a_0} \right)^{2+\alpha} - \frac{M_{bh}}{(r+r_0)} \quad (2a)$$

$$a \equiv \left(x^2 + \frac{y^2}{y_0^2} + \frac{z^2}{z_0^2} \right)^{1/2} \quad (2b)$$

where r is the galactocentric radius and the softening parameter r_0 , which has negligible effect on the results, is adopted simply to avoid numerical difficulties. The first term in the right-hand-side of equation (2a) is a softened power-law ellipsoidal potential, and the second term, negligible at radii beyond a few parsecs, is to account for the contribution to the potential by the central black hole. One could obtain a more complicated potential model based on the the density model that matches the observed luminosity profile (e.g., one based on an ellipsoidal density distribution), but the simple potential above has been adopted here for the sake of efficient force calculation.

The ellipsoidal potential is assumed to rotate with a pattern speed $\Omega_p = 50$ or $65 \text{ km s}^{-1} \text{kpc}^{-1}$, following Menzies (1990), Binney et al. (1991, 1997), Zhao et al. (1996), and Dehnen (1999). Of course, the potential in the outer bulge will not be well described with the above formula, but few inner bulge stars will have enough kinetic energy to reach the outer bulge. The masses in the outer bulge and the Galactic disk presumably have a non-negligible contribution to the potential in the inner bulge, but such contributions may be understood to be already included in parameters y_0 and z_0 in equation (2b). While Becklin & Neugebauer (1968) found the IR luminosity distribution for $r \leq 25 \text{ pc}$ to be $\sim r^{-1.8}$, the kinematic study by Lindqvist, Habing, & Winnberg (1992a) implies a density distribution in the $30 \text{ pc} \lesssim r \lesssim 100 \text{ pc}$ region proportional to $\sim r^{-1.5}$ (for $1 \text{ pc} \lesssim r \lesssim 100 \text{ pc}$, the profile becomes $\sim r^{-2.0}$). We use $\alpha = -1.8$ or -1.5 . For both a_0 and r_0 , we adopt 1 pc. The fit to the observations with the dust model of Spergel et al. (1996) gives a density aspect ratio of 1.67 (Binney, Gerhard, & Spergel 1997). We find that our potential model with $z_0 = 0.8$ gives a density aspect ratio of ~ 1.7 . We thus choose $z_0 = 0.8$ and 0.7 . For the set of parameters adopted here, the transition from X_1 orbits to X_2 orbits, which Binney et al. (1991) propose to be responsible for the 180-pc molecular ring, forms at $r \simeq 180 \text{ pc}$ only when $y_0 \geq 0.9$. Thus we adopt $y_0 = 0.9$. Finally, we choose Φ_0 such that $\Phi_0(1+r/a_0)^{2+\alpha}$ corresponds to a mass distribution with a total mass inside $r = 30 \text{ pc}$ of $8 \times 10^7 M_\odot$ (all models ex-

cept model 4; Lindqvist et al. 1992a) or $2 \times 10^8 M_\odot$ (model 4; Genzel & Townes 1987). The equipotential and isodensity contours of the above model are shown in Figure 2. The density distribution of a model with $z_0 = 0.7$ is slightly pinched at the z -axis (perpendicular to the Galactic plane). However, the calculation actually uses the derivative of the potential, and neither the potential nor its derivative has such a feature. Thus, the pinch in the density will not significantly affect our results.

2.3. Test Particles

At every 10 pc between radii of 10 and 150 pc, 300 test particles (stars) are initially distributed in the plane around a ring of that radius, making a total of 4500 stars per simulation. This discrete initial distribution allows us to apply one simulation result to initial power-law distributions of stars with various exponents by differently weighting the stars initially placed at different R . Simulation results are analyzed here for $\alpha_* = -2$ and -1 , where α_* is the exponent of the initial, power-law surface density profile of stars in the plane (R^{α_*} is a surface density profile projected along the z -axis, not along the line-of-sight). The stars' initial azimuthal angles are random. Stars initially move on X_2 orbits, and Gaussian random motions parallel and perpendicular to the plane are imposed, with standard deviations $\sigma_{v,xy} = 10\text{--}20 \text{ km s}^{-1}$ and $\sigma_{v,z} = 12\text{--}25 \text{ km s}^{-1}$, respectively. The value of 25 km s^{-1} for $\sigma_{v,z}$ is chosen to match the $\sigma_{v,z}^{GMC}$ value introduced earlier in deriving $H_{GMC} = 25 (R/150 \text{ pc})$ pc. Stars are first located at $z = 0$ and then are propagated for approximately 10 orbital periods to make the initial distribution phase-mixed. Since the dynamical relaxation time in the inner bulge is larger than the Hubble time, we neglect the interaction between stars.

2.4. Numerical Method

We have tested three numerical methods for integrating the equation of motion: the adaptive step size Runge-Kutta method, the Richardson extrapolation method (Bulirsch-Stoer method, Press et al. 1992), and the predictor-corrector method (variable time step leapfrog method; Hut, Makino, & McMillan 1995), and found that the Bulirsch-Stoer method in a rotating frame is the most efficient for our problem. We also tried Stoermer's scheme, which is for second-order conservative equations like the equation of motion without a derivative on the right-hand-side (see, e.g., Press et al. 1992), in conjunction with the Bulirsch-Stoer method, but found it to be slightly less efficient than our choice above. In our simulations, the energy of a single star is conserved to an accuracy of better than 3×10^{-6} during the entire time interval followed.

3. RESULTS

3.1. Scale Heights and Velocity Dispersions

Figure 3 shows the 3 Gyr evolution of the dispersions of vertical stellar positions and velocities for model 1. Stars initially at $30 \leq R/\text{pc} \leq 70$ and at $80 \leq R/\text{pc} \leq 120$ are separately shown. Both vertical heights and velocities significantly increase in the first 1 Gyr. The initial σ_z values are smaller for the group of stars with smaller R because the adopted potential for the bulge has a larger absolute vertical gradient at smaller R . It is interesting that the increase of vertical velocity is almost independent of R , since stars closer to the Galactic center are expected to encounter GMCs more frequently than the ones at larger distances for this model (rotational velocity is nearly independent of R and the surface density of GMCs is larger at smaller R for this model) and thus one would expect

the velocities of stars closer to the center to grow faster. We attribute this independence of vertical velocity evolution on R to the rapid evolution of the motions in the plane for stars at smaller R . Figure 4 shows the average radii in the plane, \bar{R} , for two radial groups of stars of model 1. \bar{R} of the stellar group with initially smaller R doubles and becomes comparable to that of the group with initially larger R in only 0.5 Gyr. Furthermore, we find that the average ratio of apocenter to pericenter radii of stellar orbits rapidly increases from ~ 1.5 to ~ 4 in 0.5 Gyr for both groups, and keeps increasing afterwards. Once the orbit of a star becomes highly eccentric, the star may encounter any GMC in the CMZ during its orbital motion, regardless of its initial location in the CMZ (or, regardless of its initial local number density of GMCs).

Also shown in Figure 4 is the evolution of the velocity dispersion in the plane, $\sigma_{v,xy}$, for model 1. Unlike $\sigma_{v,z}$, $\sigma_{v,xy}$ ends its rapid increase and flattens after $t \simeq 1$ Gyr. The radial velocity dispersion in the plane, $\sigma_{v,R}$, and the tangential velocity in the plane, $\sigma_{v,\theta}$, have comparable values ($0.9 \lesssim \sigma_{v,\theta}/\sigma_{v,R} \lesssim 1.1$), implying that the velocity dispersion in the plane is nearly isotropic. We also find that $\sigma_{v,z}/\sigma_{v,R}$ stays mostly between 0.7 and 0.8, which is slightly larger than the value of 0.6 found by Villumsen (1985) for the Galactic disk case.

The growth of the velocity dispersion may be described by the diffusion equation

$$\frac{d\sigma^2}{dt} \propto \sigma^{-m}, \quad (3)$$

whose solution has a functional form of

$$\sigma(t) = \sigma_0 \left(1 + \frac{t}{\tau}\right)^n, \quad (4)$$

with $n = 1/(m+2)$. When $t \gg \tau$, equation (4) simplifies to

$$\sigma(t) \propto t^n. \quad (5)$$

Villumsen (1985) found that the vertical velocity dispersion of stars in the Galactic disk is well fit by equation (4) with $n = 0.38$ ($m = 0.63$) for the first 1 Gyr, and by equation (5) with $n = 0.31$ ($m = 1.2$) for $t > 0.3$ Gyr. These values of n are only slightly larger than the theoretical estimates by Lacey (1984), 0.33 and 0.25, respectively. The theoretical estimation of these values for the inner Galactic bulge, however, is not easy because 1) the background potential is not plane-parallel, 2) the orbits of stars may not be approximated as epicyclic motions, and 3) the influence of GMCs may not be independent of each other because of their large number density and softening radius, ϵ_{GMC} . Nonetheless, a comparison of the growth rate for the bulge and the disk may be instructive. We applied non-linear, 3-parameter least squares fits (eq. [4]) to the early phase of our vertical velocity dispersion, and linear, 2-parameter least squares fits (eq. [5]) to the later data, and find that the growth rates depend on the choice of time range to fit. Model 1 shows $n = 0.30$ ($m = 1.33$) for $t \leq 1$ Gyr and $n = 0.20$ ($m = 3.0$) for $t \geq 1$ Gyr, and model 3 gives $n = 0.32$ ($m = 1.1$) and $n = 0.23$ ($m = 2.3$), respectively. As in the Galactic disk, n becomes smaller as the scattering off the GMCs drives stars farther and farther away from where the GMCs reside.

Next, we compare the evolution among different models. The velocity evolution of all our models is shown in Figure 5. Panel a) shows simulations with different bulge potential models, b) with different bulge masses inside 30 pc and pattern

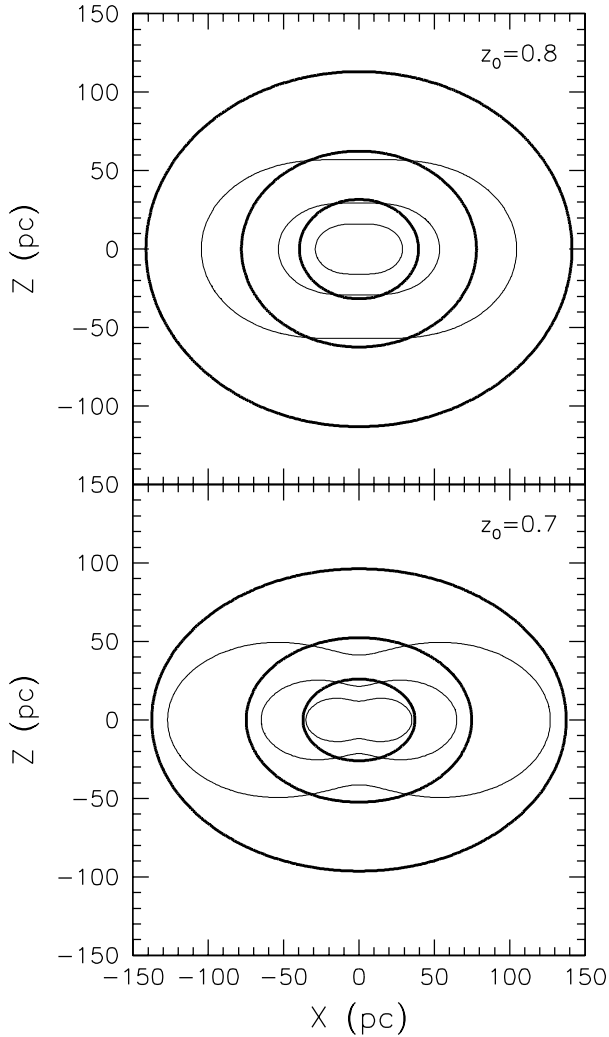


FIG. 2.— Contours of equipotential (*thick lines*) and isodensity (*thin lines*) for our bulge potential model with $z_0 = 0.8$ (model 1 [our standard model]; *upper panel*) and $z_0 = 0.7$ (model 2; *lower panel*). Contours are drawn at linear steps for the potential and logarithmic steps for the density. The x-axis lies in the Galactic plane and the z-axis is perpendicular to the plane.

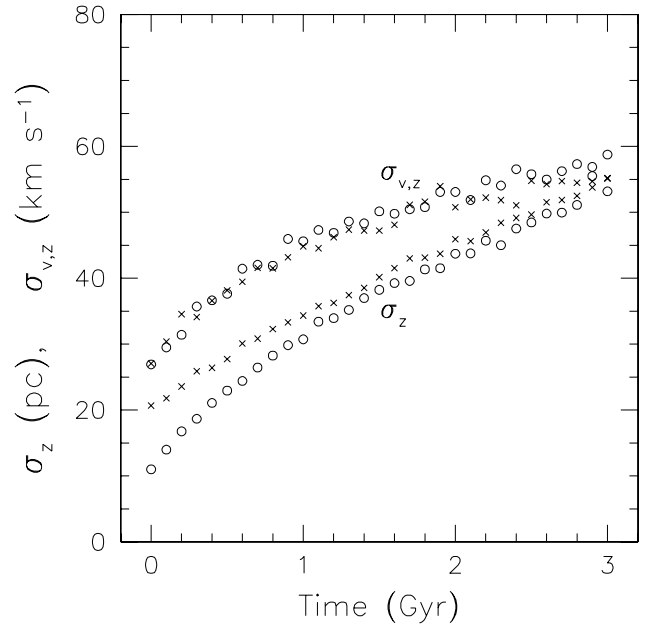


FIG. 3.— Evolution of dispersions of z-axis stellar positions and velocities for model 1. Stars initially located at $30 \leq R/\text{pc} \leq 70$ (*circles*) and $80 \leq R/\text{pc} \leq 120$ (*crosses*) are separately presented.

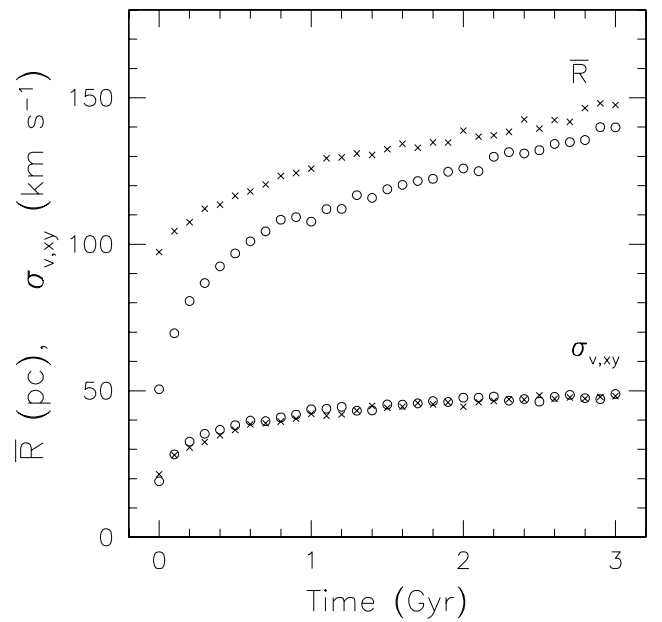


FIG. 4.— Evolution of the average R values and the velocity dispersion in the plane for model 1. Symbols have the same meaning as in Figure 3.

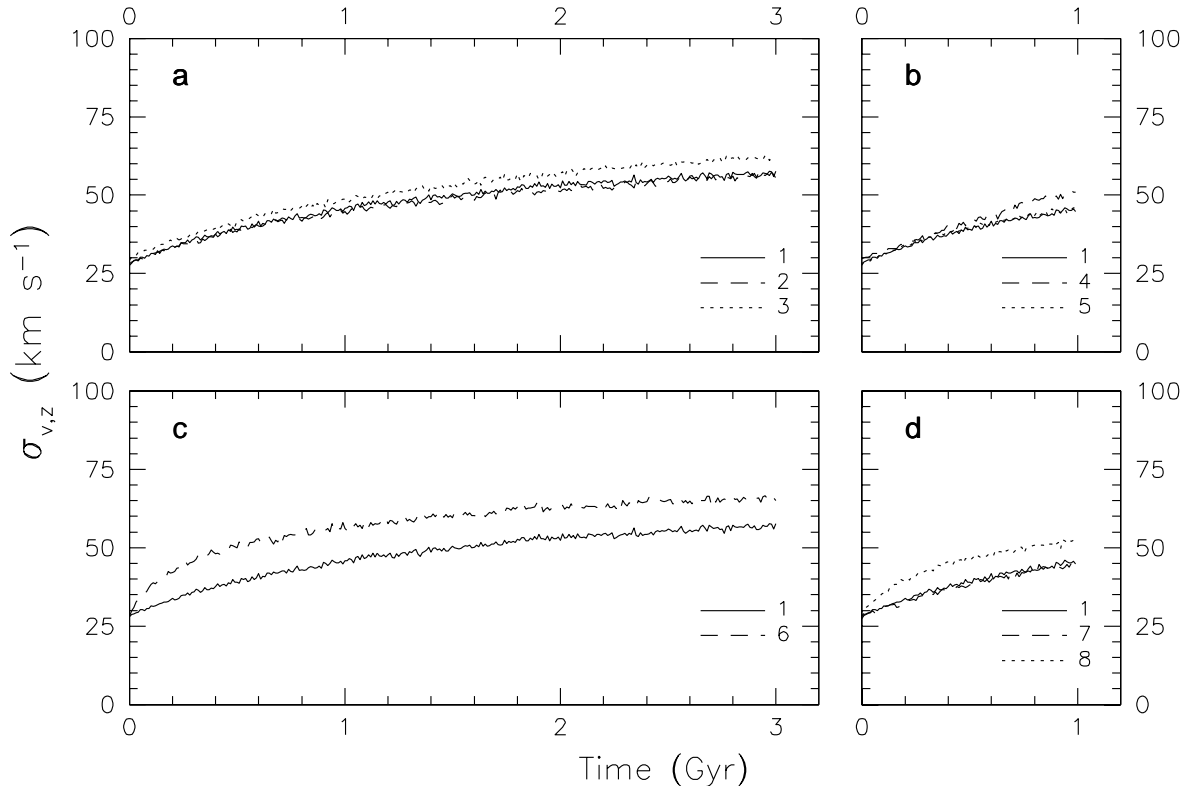


FIG. 5.— Evolution of vertical velocity dispersion. a) models 1, 2, and 3 (different Galactic potential models); b) models 1, 4, and 5 (different bulge masses and pattern speeds); c) models 1 and 6 (different GMC masses); and d) models 1, 7, and 8 (different GMC distribution and sizes).

speeds, c) with different GMC masses, and d) with different GMC distributions and sizes. Panels a) and b) show that in general, the vertical velocity evolution is not sensitive to the parameters used to model the bulge. The heating is only slightly more efficient when the potential is shallower (larger α).

On the other hand, panels c) and d) of Figure 5 illustrate that the vertical velocity evolution is dependent on the mass and size of GMCs, but not on the distribution of GMCs. Stars are found to have highly eccentric orbits, which allows them to encounter any GMC in the CMZ. Thus the heating rate is determined mostly by the total number and mass of the GMCs in the CMZ, and not by the distribution of GMCs.

Although not shown in Table 1 and Figure 5, we have tried other initial stellar velocity dispersions ($\sigma_{v,xy} = 10 \text{ km s}^{-1}$ and $\sigma_{v,z} = 12 \text{ km s}^{-1}$), but found no significant difference from our standard model. The velocity dispersions rapidly increase by a factor of a few in the early phase, so unless the initial velocities are different by an order of magnitude, any initial difference in velocity dispersions that is smaller than the amount of increase in the early phase will soon be indistinguishable.

3.2. Density Profiles and Aspect Ratios

In this subsection, we discuss quantities with which we may more directly assess the hypotheses that the r^{-2} cluster is a result of sustained star formation in the CMZ and that the GMCs are responsible for the vertical diffusion of newborn stars. To do so, we project the simulation stars onto the l - b plane of the sky and compare them with observations of a certain stellar type. From a variety of models of the inner Galaxy, the major axis of the bulge bar potential has been found to have an angle of

15 – 30° to the east from the line connecting the Galactic center and the Sun (Binney et al. 1997, among others). Here we adopt 20° .

Our simulations initially have an equal number of stars for each linear R bin, making the exponent of the radial profile of the initial surface density of simulation stars in the plane, α_* , equal to -1 (note that α_* is different from α , the exponent for the bulge density profile). However, by properly weighting the stars in each bin, one may construct volume and projected (along the line-of-sight) surface density profiles (we denote the latter with Σ) for different α_* values. Figure 6 shows the Σ profile along the l and b axes at several epochs for $\alpha_* = -2$. It is interesting that Σ along the l axis gradually decreases at $l < 30$ pc while maintaining its overall profile. The Σ profile along the b axis experiences a significant flattening in its power-law slope.

Plotted in Figure 7 is the evolution of the best-fit power-law exponent for the Σ profile between 10 and 100 pc along the l and b axes. As anticipated from Figure 6, while the l axis slope does not vary much, that along the b axis continuously increases and approaches the former at the end of the simulation. The slope values for the $\alpha_* = -2$ case are steeper than those for the $\alpha_* = -1$ case by ~ 0.5 (when the distribution extends to infinity, a difference of 1 in α_* should result in a difference of 1 in the power-law Σ slopes; however, the stellar distribution in our simulations, as in reality, is finite, so the relation between α_* and the Σ slope is not as strong as in the infinite case). Using a circular aperture, Becklin & Neugebauer (1968) obtained integrated near-infrared intensities of the inner Galactic bulge region as a function of aperture size and derived a surface intensity profile (projected along the line-of-sight) proportional to

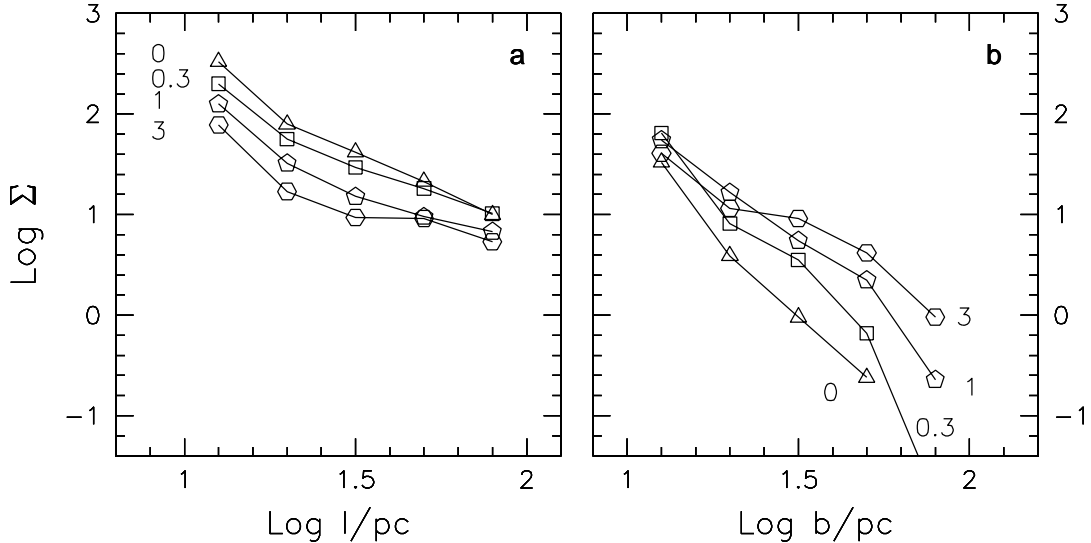


FIG. 6.— Surface density profiles (projected along the line-of-sight) for model 1 along the l axis (a) and along the b axis (b) at four epochs, 0, 0.3, 1, and 3 Gyr. Stars that are less than 10 pc away from the axes are considered. The numbers in the plot denote the time in Gyr. Σ is in arbitrary units. The angle between the major axis of the bar and the Sun-Galactic center line is assumed to be 20° , and $\alpha_* = -2$ is adopted. The $1\text{-}\sigma$ Poisson error in $\log \Sigma$ is smaller than 0.05 octave except for $\log \Sigma < 0$.

$r^{-0.8}$. The enclosed mass in the $5 \lesssim r/\text{pc} \lesssim 100$ region obtained by Lindqvist et al. (1992a) also implies a surface density profile of $\propto r^{-0.8}$. On the other hand, by fitting an ellipse with an aspect ratio of 2.2 to the distribution of stars with dereddened, apparent K mag between 5 and 6 (Haller & Rieke 1999 estimate such stars to be a few 10^8 yr old), Catchpole et al. (1990) obtained a steeper exponent, -1.4 , after correcting for the disk contamination, crowding, and dark clouds. The invariance of the l -axis slope over time in our simulations makes the l -axis slope indicative of its original slope. From Figure 7, we find that the deprojection of our simulation with $\alpha_* = -1$ approximately reproduces the slope obtained by Becklin & Neugebauer and Lindqvist et al., and that with $\alpha_* = -2$ gives the slope obtained by Catchpole et al. In any case, it appears reasonable to assume that the time-averaged star formation efficiency in the inner bulge has a dependence between R^{-2} and R^{-1} in the plane.

Finally, we compare the vertical thickening of our simulation stars with the observations. Since it is more instructive to compare with the observation of a coeval population (otherwise, the overlap of populations of different ages would blend out the age dependence of a certain quantity), we use the OH/IR stars observed by Lindqvist et al. (1992b) in the inner bulge (total number of 134). One of the measures of the thickness or flatness of a distribution is the aspect ratio of major (l) to minor (b) axes. However, the aspect ratio itself can be defined in several ways. Catchpole et al. (1990) measured the aspect ratio of the stellar distribution using observed isodensity contours. However, we find that a distribution of 134 stars is too sparse to obtain meaningful contours. For this reason, we determine the aspect ratio as the ratio of the major to minor axes of an ellipse which best fits the distribution of stars projected onto the plane of the sky. The best-fit ellipse was taken to be that for which the area per unit angle, taken as a function of angle on the sky measured from the center of the ellipse, was best matched by the function describing the number of stars per unit angle. The binning utilized to determine the latter function was chosen to

ensure a statistically large number of stars in each angular bin. The orientation of the major axis of the fitted ellipse was fixed at the orientation of the Galactic plane. This is a one-dimensional fit, thus is less sensitive to the density profile, which is not a primary concern here. The observation by Lindqvist et al. was constrained to a cross-shaped area, but we limit the calculation of the aspect ratio of both observations and simulations to the stars in the $200\text{ pc} \times 80\text{ pc}$ area positioned at the Galactic center (the number of OH/IR stars observed by Lindqvist et al. in this area is 124). We here assume $\alpha_* = -2$, but we find that $\alpha_* = -1$ gives nearly the same aspect ratios.

Figure 8 shows the evolution of the aspect ratios of all models. The evolution is noticeably dependent only on the mass and size of GMCs as well as the bulge mass. The former dependence is a naturally expected phenomenon, and the latter dependence appears to be due to an initially larger aspect ratio of model 4, which has a larger vertical potential gradient, but the same initial vertical velocity dispersion as the other models.

In spite of the dependence on the GMC parameters, all models except model 4 (larger bulge mass case) evolve to having aspect ratio values below 3 in 1–2 Gyr. The same elliptical fit to the distribution of observed OH/IR stars in the central $200\text{ pc} \times 80\text{ pc}$ area gives an aspect ratio of $2.6^{+0.5}_{-0.5}$ (super- and subscripts denote 95 % confidence limits), shown in Figure 8 as a horizontal dashed line. Based on the observed bolometric magnitudes of the OH/IR stars ($M_{bol} \simeq -5$; Jones et al. 1994 & Blommaert et al. 1998) and the theoretical initial mass-bolometric magnitude relation of Vassiliadis & Wood (1993), Sjouwerman et al. (1999) estimates OH/IR stars in the inner bulge to be 1–2 Gyr old. Since the time scale for an initially flattened stellar population to achieve an aspect ratio of the observed OH/IR stars agrees well with the estimated age of the OH/IR stars, we conclude that scattering by the GMCs is one of the predominant mechanisms, perhaps the most important mechanism, for the vertical diffusion of stars in the inner Galactic bulge.

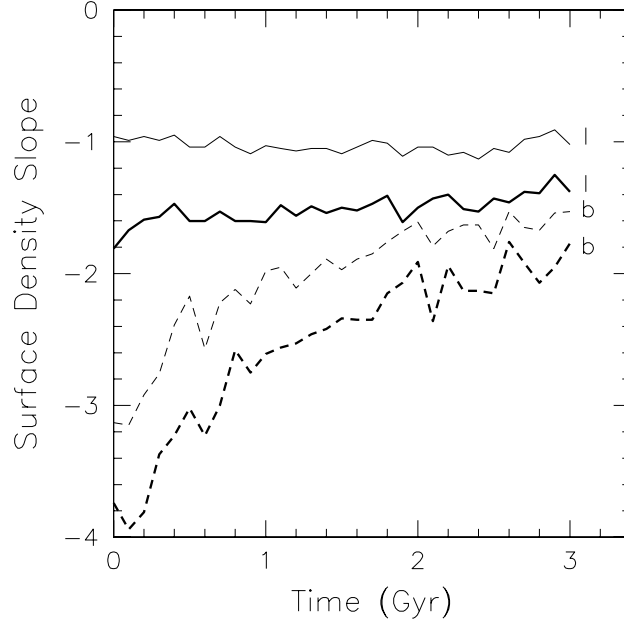


FIG. 7.— Evolution of the surface density slope (projected along the line-of-sight) for model 1 along the l axis (solid lines) and along the b axis (dashed lines). The slopes are the best-fit power-law exponent to the distributions obtained in Figure 6. The slopes are calculated for the $\alpha_* = -2$ case (thick lines) and the $\alpha_* = -1$ case (thin lines).

It has been suggested by Baud et al. (1981) that the expansion velocity of the circumstellar shell of an OH/IR star, v_{exp} , is a good statistical age indicator. For the Galactic inner bulge, Lindqvist et al. (1992a) confirmed this correlation by showing that the OH/IR stars there with $v_{exp} \geq 18 \text{ km s}^{-1}$ have younger kinematical and morphological characteristics than the ones with $v_{exp} < 18 \text{ km s}^{-1}$. Our aspect ratio calculation for the same sample finds that such a division is clearer when the division is made at 20 km s^{-1} : while the aspect ratio of stars with $v_{exp} \leq 20 \text{ km s}^{-1}$ is $2.5^{+0.5}_{-0.4}$, that of stars with $v_{exp} > 20 \text{ km s}^{-1}$ is $3.2^{+1.6}_{-1.3}$. Although the latter, which is calculated from a sample of only 29, is rather uncertain, the rapid decrease of aspect ratios in our simulations supports the notion that the former group is younger than the latter group.

Another measure for the comparison between our simulations and observations is the root-mean-square (rms) value of the Galactic height (z_{rms}). This is also a projected quantity, but is sensitive to the vertical evolution of stars. We limit the calculation of z_{rms} to stars with $|l| < 20 \text{ pc}$ and $|b| < 80 \text{ pc}$, in order to minimize the effects of planar evolution and of a few outliers with very large $|z|$ values. The evolution of z_{rms} for all models is shown in Figure 9 along with the z_{rms} value for the OH/IR stars in the same region, 22 pc (thick dashed lines). The figure is made assuming $\alpha_* = -2$, but we find that $\alpha_* = -1$ typically gives only 10–20 % larger z_{rms} values. All models, probably except model 4, reach the value for the OH/IR stars within $\sim 2 \text{ Gyr}$, as in the case of the aspect ratio evolution. One noticeable behavior difference between z_{rms} and the aspect ratio is its largely different convergent values between models 1 and 6. Thus, z_{rms} could be useful in comparing simulations with the observed distribution of stars older than OH/IR stars.

4. DISCUSSION

The surface density profile along the l axis of model 1 at 3 Gyr (Fig. 6a) shows a nearly flat slope near $l = 30 \text{ pc}$. We

find that this is caused by a relatively shallow volume density profile in the plane between $r = 30 \text{ pc}$ and 100 pc , $\rho \sim r^{-1}$ (see Fig. 10). In the case of model 3 (shallower bulge potential), the volume density profile becomes even shallower than r^{-1} at 3 Gyr. However, the profile of model 7, where the GMC distribution is uniform over R , does not change much over its simulation period, 1 Gyr. Thus the shallow density profiles shown in $\alpha_{GMC} = -1$ models are attributable to the relatively larger abundance of GMCs at smaller R , which more efficiently depletes stars in that region by heating. It is difficult to estimate the current volume density profiles in the inner bulge, both observationally and from our simulations. Observationally, we only have projected surface density profiles and limited radial velocity information. To estimate the density profile from our simulations, one needs to assume a star formation history and a radial dependence of the star formation in the inner bulge. Until these are better understood, simulations may not give a strong constraint to the density profile. However, our simulations still seem to be able to suggest that the local density in the plane between 30 and 100 pc may be as shallow as or close to r^{-1} (compared to $r^{-1.8}$ obtained by Becklin & Neugebauer 1968 for $r < 25 \text{ pc}$ and $r^{-2.5}$ by Lindqvist et al. 1992a for $1 < r/\text{pc} < 10$). Such shallow profiles may carry important implications for star formation in the inner bulge, since a sphere (the inner bulge in this case) with a volume density profile close to r^{-1} has negligible tidal forces in it (the r^{-1} density profile gives no tidal forces; if the density drop is shallower than r^{-1} , the tidal force even becomes compressive). Thus if the local volume density in the inner bulge can be indeed shallower than, say, $r^{-1.5}$, formation of stars there may not be as difficult as has been speculated (the galactic tidal field acts against the collapse or contraction of molecular clouds into a star). The enclosed mass as a function of galactocentric radius deduced by Lindqvist et al. (1992a; Fig. 10) shows a steep increase (thus shallow decrease in density) between 30 and 100 pc (steeper than $\sim r^{-1.5}$, implying a

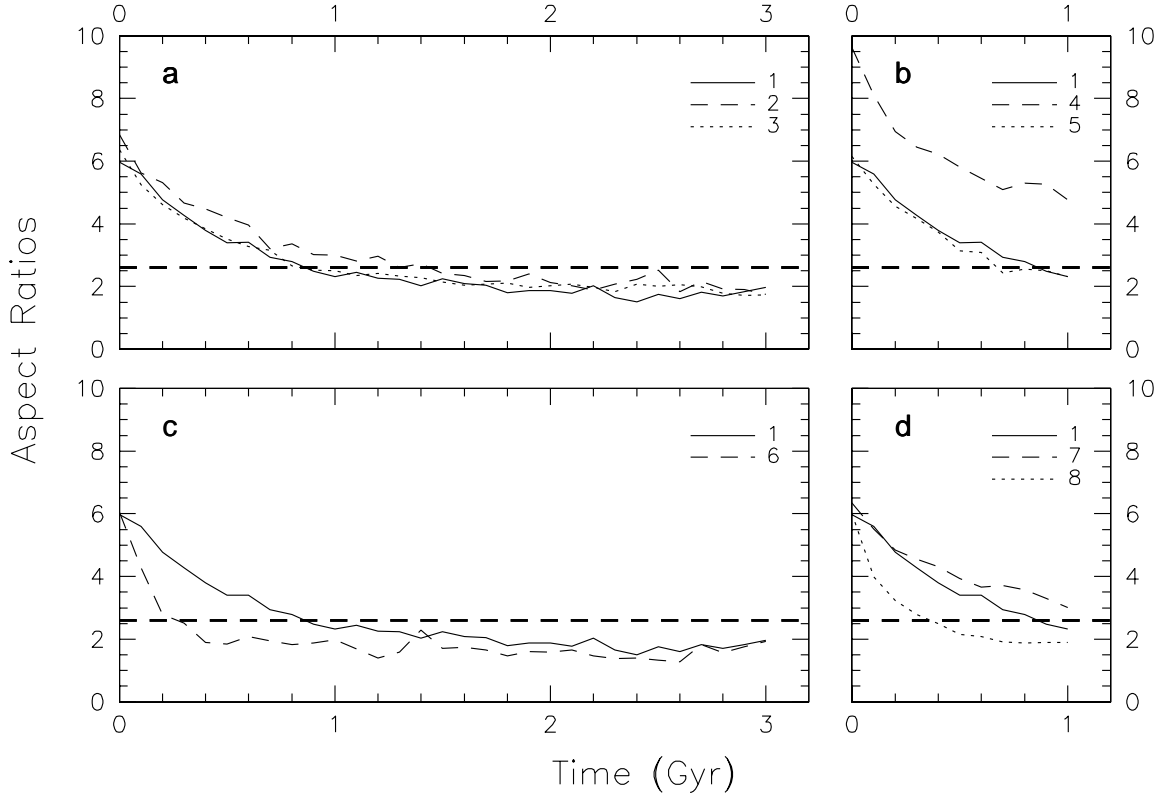


FIG. 8.— Evolution of aspect ratios of our models. See the caption of Figure 5 and Table 1 for the description of each panel. See text for our definition of aspect ratio. The horizontal dashed line indicates the aspect ratio from the distribution of OH/IR stars observed by Lindqvist et al. (1992). $\alpha_* = -2$ is adopted. The 95 % confidence limit for the observed aspect ratio is $2.6^{+0.5}_{-0.5}$.

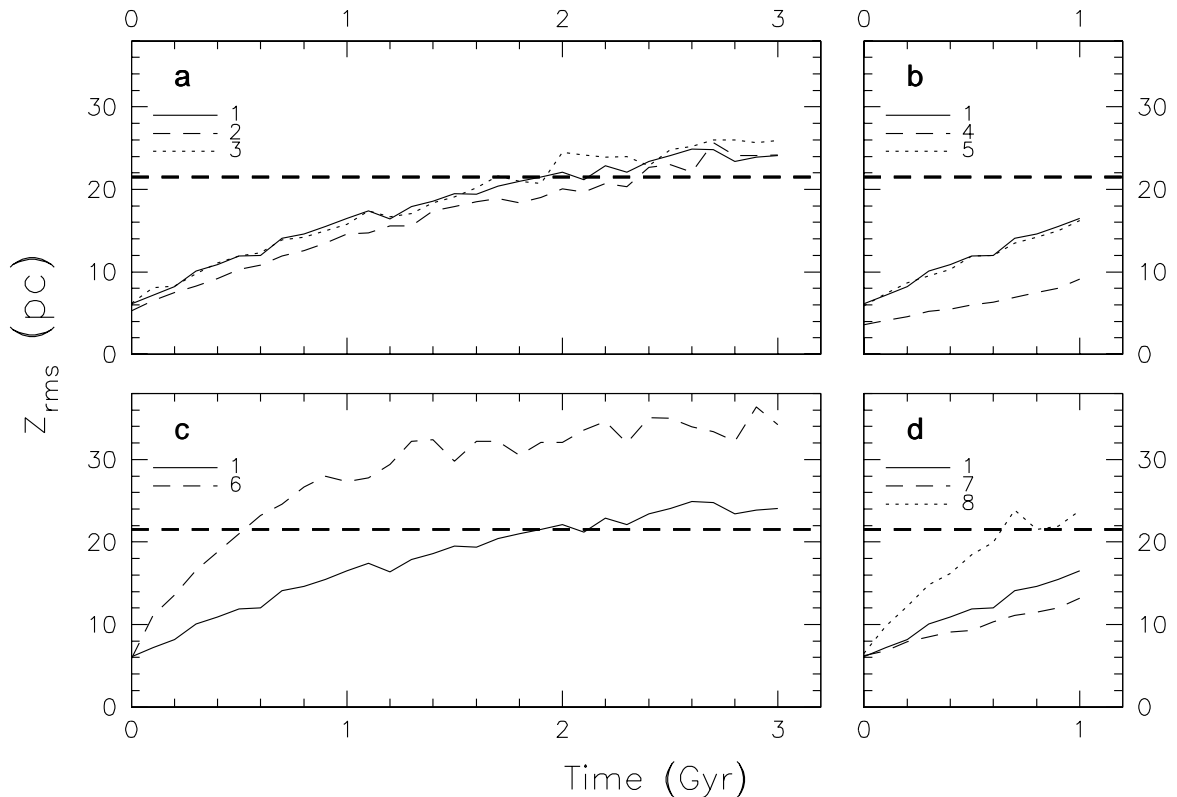


FIG. 9.— Evolution of the root-mean-square value of the Galactic height, z_{rms} , from our simulations. The calculation of z_{rms} is limited to stars with $|l| < 20$ pc and $|b| < 80$ pc. See the caption of Figure 5 and Table 1 for the description of each panel. The horizontal dashed line indicates the z_{rms} value from the distribution of OH/IR stars observed by Lindqvist et al. (1992). $\alpha_* = -2$ is adopted. The $2\text{-}\sigma$ uncertainty level for z_{rms} values is less than 10 %.

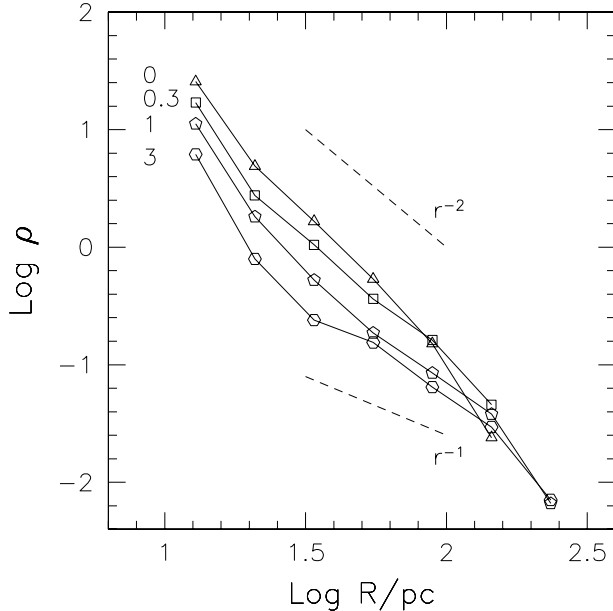


FIG. 10.— Volume density profiles in the plane, ρ , for model 1 at four epochs, 0, 0.3, 1, and 3 Gyr. Stars that are less than 10 pc away from the plane are considered. The numbers in the plot denote the time in Gyr, and dashed lines indicate profiles of r^{-1} and r^{-2} . ρ is in arbitrary units. $\alpha_* = -2$ is adopted. The 1- σ Poisson error is smaller than 0.05 octave.

density profile shallower than $r^{-1.5}$), and this supports our simulation results that the density profile becomes shallower in the $30 \lesssim r/\text{pc} \lesssim 100$ region and also supports the above discussion on the possibly favorable star formation environment there.

Considering the age of the Galaxy, OH/IR stars in the inner bulge are relatively young. Our comparison with a “young” population strongly supports our hypothesis that the GMCs are responsible for the vertical diffusion, but does not necessarily imply that the entire r^{-2} stellar population is a result of sustained star formation in the CMZ. To address this issue, one needs to account for the evolution and accumulation of stellar populations over the lifetime of the Galaxy. Since the evolution of aspect ratios in Figure 8 appears to converge to an asymptotic value at times $\gtrsim 2$ Gyr, we may expect that the agglomeration of stars formed in the CMZ over the lifetime of the Galaxy will have a stellar distribution not much different from that of the last stages of our simulations. A systematic observation that covers the full inner bulge region with good resolution and sensitivity is needed to take the next step in this analysis. This need may be fulfilled by the currently ongoing 2MASS survey.

5. SUMMARY

We have performed numerical simulations of scattering of young stars off the GMCs in the inner bulge. Several different bulge potentials, GMC models and distributions, and initial conditions of the stellar population have been considered.

First we find that when $\alpha_{GMC} = -1$, the stars inside ~ 70 pc experience rapid radial diffusion in the plane during the early phase. The consequences of this are that 1) later evolution of the inner stars is very similar to that of the outer stars (initial $R \gtrsim 80$), and 2) the depletion of stars in the inner region makes the volume density profile in the plane between 30 and 100 pc quite shallow (possibly close to r^{-1}). The latter is supported by the rapid increase in the enclosed mass between 30 and 100 pc (Lindqvist et al. 1992a), and implies that the tidal forces in

that region may not be as hostile to star formation as has been previously conjectured.

After a rapid initial rise during the first ~ 0.5 Gyr, especially for the inner stars, \bar{R} linearly increases afterwards (in case of model 1, \bar{R} reaches 150 pc in ~ 3 Gyr). The vertical positional dispersion of stars, on the other hand, grows almost linearly for the whole computational interval (model 1 reaches $\sigma_z = 50$ pc at ~ 3 Gyr).

The projected surface density of test stars along the galactic plane inside 100 pc decreases as stars diffuse out both radially and vertically, but roughly maintains its initial slope over our simulation period. On the other hand, the slope of the projected surface density profile along the b (vertical) axis becomes significantly shallower during the same period and makes the overall stellar population rounder.

The comparison between observations and our simulations of the l -axis surface density profile (projected along the line-of-sight) in the $10 \lesssim r/\text{pc} \lesssim 100$ region suggests that newborn stars have an initial surface density profile (projected along the z -axis in the plane) of $R^{-2} - R^{-1}$. However, the estimation of 3-dimensional structure from 2-dimensional observation requires more careful study in the context of non-axisymmetric stellar models in order to reveal the true volume density profile in the inner bulge.

The aspect ratios of our young stellar configuration are initially larger than 6, but the ratios become smaller than 3 in 1–2 Gyr, except for one model. This is because the scattering off GMCs diffuses stars preferentially in the vertical direction (since the density gradient is greater in that direction), except in the very early phase. The aspect ratios converge to values between 1.5 and 2.5 in 1–2 Gyr. Since OH/IR stars in the inner bulge, which are estimated to be 1–2 Gyr old (Sjouwerman et al. 1999), have an aspect ratio of 2.6, we conclude that scattering by the GMCs is one of the predominant mechanisms, and possibly the most important for the vertical diffusion of stars in

the inner Galactic bulge.

S.S.K. is grateful to Jongsoo Kim and Kwang-II Seon for help with computer facilities, and to Burkhard Fuchs, Cheongho Han, Chang Won Lee, Hyung Mok Lee, Douglas Lin, David Merritt, William Newman, and Roland Wielen

for valuable discussions. We also appreciate the comments of an anonymous referee, which significantly improved our manuscript. This work was supported in part by the International Cooperative Research Program of the Korea Research Foundation to Seoul National University in 1999, and in part by a NASA grant to UCLA.

REFERENCES

- Barbanis, B., & Woltjer, L. 1967, *ApJ*, 150, 461
 Baud, B., Habing, H. J., Matthews, H. E., & Winnberg, A. 1981, *A&A*, 95, 156
 Becklin, E. E., & Neugebauer, G. 1968, *ApJ*, 151, 145
 Binney, J., Gerhard, O. E., Stark, A. A., Bally, J., & Uchida, K. I. 1991, *MNRAS*, 252, 210
 Binney, J., Gerhard, O., & Spergel, D. 1997, *MNRAS*, 288, 365
 Blommaert, J. A. D. L., van der Veen, W. E. C. J., Van Langevelde, H. J., Habing, H. J., & Sjouwerman, L. O. 1998, *A&A*, 329, 991
 Carlberg, R. G., & Sellwood, J. A. 1985, *ApJ*, 292, 79
 Carlberg, R. G. 1987, *ApJ*, 322, 59
 Catchpole, R. M., Whitelock, P. A., & Glass, I. S. 1990, *MNRAS*, 247, 479
 Contopoulos, G., & Mertzaniades, C. 1977, *A&A*, 61, 477
 Dehnen, W. 1999, *ApJ*, 524, L35
 Evans, N. W., & de Zeeuw, P. T. 1994, *MNRAS*, 271, 202
 Genzel, R., & Townes, C. H. 1987, *ARA&A*, 25, 377
 Haller, J. W., & Rieke, M. J. 1989, in *Proc. of IAU Symp. 136, The Center of the Galaxy*, ed. M. Morris (Dordrecht: Kluwer), 487
 Hut, P., Makino, J., & McMillan, S. 1995, *ApJ*, 443, L93
 Hüttemeister, S., Wilson, T. L., Bania, T. M., & Martin-Pintado, J. 1993, *A&A*, 280, 255
 Jenkins, A., & Binney, J. 1990, *MNRAS*, 245, 305
 Jenkins, A., & Binney, J. 1994, *MNRAS*, 270, 703
 Jones, T. J., McGregor, P. J., Gehr, R. D., & Lawrence, G. F. 1994, *AJ*, 107, 1111
 Kent, S. M., Dame, T. M., & Fazio, G. 1991, *ApJ*, 378, 131
 Lacey, C. G. 1984, *MNRAS*, 208, 687
 Lindqvist, M., Habing, H. J., & Winnberg, A. 1992a, *A&A*, 259, 118
 Lindqvist, M., Winnberg, A., Habing, H. J., & Matthews, H. E. 1992b, *A&AS*, 92, 43
 Menzies, J. W. 1990, in *Proc. of ESO/CTIO Workshop on Bulges of Galaxies (Garching)*, 115
 Morris, M. 1996, *IAU Symp. No. 169, Unsolved Problems of the Milky Way*, L. Blitz, P. J. Teuben, eds. (Dordrecht: Kluwer), 247
 Morris, M. 1997, in *Proc. of IAU Symp. 170, CO: Twenty-five Years of Millimeter-Wave Spectroscopy*, eds. W. B. Latter et al. (Dordrecht: Kluwer), 57
 Morris, M., & Serabyn, E. 1996, *ARA&A*, 34, 645
 Oka, T., Hasegawa, T., Hayashi, M., Handa, T., & Sakamoto, S. 1998, *ApJ*, 493, 730
 Press, W. H., Teukolsky, S. A., Vetterling, W. T., & Flannery, B. P. 1992, in *Numerical Recipes in FORTRAN* (Cambridge: Cambridge University Press)
 Sellwood, J. A., & Kahn, F. D. 1991, *MNRAS*, 250, 278
 Serabyn, E., & Morris, M. 1996, *Nature*, 382, 602
 Sjouwerman, L. O., Habing, H. J., Lindqvist, M., van Langevelde, H. J., & Winnberg, A. 1999, in *The Central Parsecs of the Galaxy, ASP Conf. Ser. vol. 186*, eds. H. Falcke, A. Cotera, W. J. Duschl, F. Melia, & M. J. Rieke, p. 379
 Spergel, D. N., Malhotra, S., & Blitz, L. 1996, unpublished work (see Binney, Gerhard, & Spergel 1997)
 Spitzer, L., & Schwarzschild, M. 1951, *ApJ*, 114, 385
 Spitzer, L., & Schwarzschild, M. 1953, *ApJ*, 118, 106
 Stark, A. A., Gerhard, O. E., Binney, J., & Bally, J. 1991, *MNRAS*, 248, 14p
 Vassiliadis, E., & Wood, P. R. 1993, *ApJ*, 413, 641
 Villumsen, J. V. 1983, *ApJ*, 274, 632
 Villumsen, J. V. 1985, *ApJ*, 290, 75
 Weiland, J. L., et al. 1004, *ApJ*, 425, L81
 Weinberg, M. D. 1994, *ApJ*, 421, 481
 Wielen, R. 1977, *A&A*, 60, 263
 Zhao, H., Rich, R. M., & Biello, J. 1996, *ApJ*, 470, 506